Anjali A. Ingle, Diwakar Z. Shende, Kailas L. Wasewar* and Aniruddha B. Pandit

Performance of Pd catalyst supported on trimetallic nanohybrid Zr–Al–La in hydrogenation of ethylanthraquinone

https://doi.org/10.1515/ijcre-2021-0271
Received November 1, 2021; accepted April 13, 2022;
published online May 10, 2022

Abstract: In light of the recent COVID-19 pandemic, the demand for hydrogen peroxide has increased significantly due to its widespread use in disinfectant formulations. The present study aims to develop an efficient nanohybrid material as catalyst support for the successful hydrogenation of ethylanthraquinone for the production of hydrogen peroxide. Co-precipitation and wet impregnation methods were used to prepare nanohybrid Zr–Al–La supported Pd catalyst (Pd/Zr–Al–La). The high surface area (146.56 m^2/g) of Zr–Al–La makes it suitable to use as support and causes to lower the mass transfer resistance and dispersion of active metal. XRF, BET, FTIR, and TGA were used to characterize the developed catalyst. The catalytic activity of the developed catalyst was studied using a high-pressure autoclave reactor to obtain a notable yield of H_2O_2 as 93.8% at 75 °C, 0.3 MPa, and 0.5 g of catalyst dose, a significant enhancement over the traditional Pd catalyst with Al_2O_3 support (63%) with the loss of active quinone compound. The mass transfer limitation of the reaction is high using only a Pd catalyst. The calculated mass transfer resistance of the reaction over Pd/Zr–Al–La catalyst was found to be moderate with a diffusion coefficient of the reactant (H_2) as 0.0133×10^{-6} m^2/s at 75 °C. It was also verified and confirmed with the Thiele modulus (calculated as 0.0314), no mass transfer resistance. The effectiveness factor (η_s) was found to be 1.0, indicating the negligible mass transfer resistance in the hydrogenation reaction using Pd/Zr–Al–La catalyst.

Keywords: hydrogenation of ethylanthraquinone; palladium catalyst; trimetallic nanohybrid support (Zr–Al–La).

***Corresponding author: Kailas L. Wasewar**, Advanced Separation and Analytical Laboratory (ASAL), Department of Chemical Engineering, Visvesvaraya National Instutute of Technology, Nagpur-440010, Maharashtra, India, E-mail: k_wasewar@rediffmail.com. https://orcid.org/0000-0001-7453-6308
Anjali A. Ingle and Diwakar Z. Shende, Advanced Separation and Analytical Laboratory (ASAL), Department of Chemical Engineering, Visvesvaraya National Instutute of Technology, Nagpur-440010, Maharashtra, India, E-mail: anjuingle2013@gmail.com (A.A. Ingle), diwakar.shende@gmail.com (D.Z. Shende).
https://orcid.org/0000-0002-9967-5598 (A.A. Ingle)
Aniruddha B. Pandit, Department of Chemical Engineering, Institute of Chemical Technology, Mumbai-400019, India,
E-mail: ab.pandit@ictmumbai.edu.in

1 Introduction

Hydrogen peroxide (H_2O_2) is the most promising oxidant for clean and environmentally safe chemical processes since it does not produce any harmful compounds (Campos-Martin, Blanco-Brieva, and Fierro 2006; Garcia-Serna et al. 2014; Gema et al. 2016; Han et al. 2015; Melada et al. 2006; Tan et al. 2012; Yao et al. 2016). H_2O_2 has been used as an antiseptic since late 1800s, and its mechanisms of action have been extensively studied. Further, in light of the recent COVID-19 pandemic, the demand for H_2O_2 has been increased significantly due to its widespread use in disinfectant formulations and therapeutic uses. Many medical practioners have reported utilizing H_2O_2 successfully against COVID-19 in various modalities around the world (Trejo et al. 2021). H_2O_2 may have preventative and therapeutic benefits in the COVID-19 pandemic due to its anti-infective and oxygenating capabilities. The anthraquinone (AQ) process is the most common way of producing H_2O_2 (Campos-Martin, Blanco-Brieva, and Fierro 2006). It involves a cyclic procedure in which alkyl-anthraquinone (AAQ) is hydrogenated to alkyl-anthrahydroquinone (AAHQ) using the Pd catalyst. The formation of H_2O_2 and the regeneration of AAQ occur followed by the oxidation of AAHQ (Campos-Martin, Blanco-Brieva, and Fierro 2006; Han et al. 2015; Yao et al. 2016). Due to its exceptional solubility in water, H_2O_2 is extracted from the mixture using water as a solvent to recover H_2O_2 of various strengths up to 50% concentration as an aqueous solution (Cheng et al. 2008; Fang et al. 2005). Figure 1 describes the reaction system for H_2O_2 production.

The AQ process is the basic and widely used method for the production of H_2O_2 in the world. The other synthesis processes for H_2O_2 include the direct reaction of H_2 and O_2 using a hydrogenation catalyst (Chen et al. 2013; Paparatto

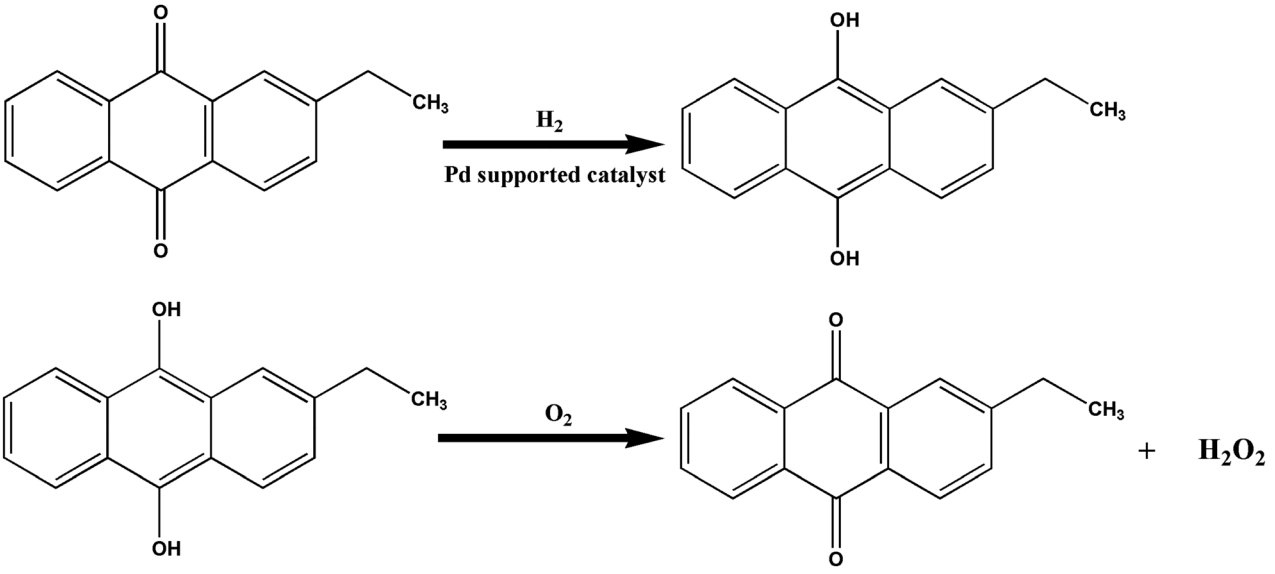

Figure 1: Hydrogen peroxide production by the AQ process.

and D'Aloisio 2003), photo-catalytic reactions over semiconductor oxides (Gabriele et al. 2003), and the synthesis using $CO/O_2/H_2O$ mixtures in presence of metal complexes (Zudin, Likholobov, and Yermakov 1980). However, there is the risk of explosion with these systems, alongwith the drawbacks of low H_2O_2 concentrations. The AQ process overcomes disadvantages of the high energy consumption and production costs due to its larger scale production and higher concentration of H_2O_2. Also, it is advantageous over all the commercial processes with mild reaction temperatures and higher production rates. Over the last decade, the advancements in slurry reactor technology and catalysts have sparked industrial interest and academic research in the AQ process. The researchers have used highly active and selective catalysts for the hydrogenation of ethylanthraquinone (EAQ) for the synthesis of H_2O_2 using the AQ process with various types of reactors. Another interesting approach is to use an autoclave reactor to provide the broad gas-liquid contact area and homogeneous mixing of the reactants (Hong et al. 2017; Ingle et al. 2020a, 2020b; Ingle, Shende, and Wasewar 2021; Li et al. 2021; Ma et al. 2019; Yuan et al. 2016, 2017a, 2017b; Zhang et al. 2017). The hydrogenation of EAQ using Pd catalyst is governed by the mass transfer process, with fast reaction. Therefore, the catalyst, its nanostructured support, and surface morphology must be optimized to minimize the mass transfer resistance.

The effectiveness of a catalyst can be improved with suitable tailoring of the morphology and the composition of supporting materials. The scientific community has been quite interested in recent research on the topic of mixed oxide supports. The oxides ZrO_2-Al_2O_3 have been investigated as catalyst supports for EAQ hydrogenation (Tang et al. 2014). The effects of lanthanum addition on Ni-B/γ-Al_2O_3 amorphous alloy catalysts used in EAQ hydrogenation were investigated by Hou et al. (2004). It was discovered that adding various metal oxides to existing supports increases the catalyst's selectivity. Researchers have employed nanohybrid supported catalysts (bimetallic and trimetallic) for a variety of hydrogenation processes (Adams et al. 2007; Carvalho et al. 2004; Chen et al. 2015; Hungria et al. 2006; Liew et al. 2019; Surisetty, Dalai, and Kozinski 2010; Toshima et al. 2007).

The nanohybrid trimetallic support Zr–Al–La was employed as the Pd support in the present study to synthesize Pd/Zr–Al–La catalyst. The procedure for preparing the support was followed as specified in our previous publication (Ingle et al. 2020b). The co-precipitation technique was employed to prepare a new nanohybrid trimetallic support as Zr–Al–La, followed by impregnation with Pd using the incipient wet impregnation method. The co-precipitation by direct contact of oxide supports are gaining the scientific interest due to its accessibility and low cost. Because EAQ possesses electrophilic characteristics, and the synthesized catalyst with the nucleophilic reagent for the carbonyl groups in the EAQ structure, the Pd/Zr–Al–La catalyst has high hydrogenation efficiency (Shen et al. 2011). It can provide higher hydrogenation efficiency due to the higher electron density as a result of adsorption of electrophilic EAQ and nucleophilic Pd catalyst together. To investigate the characteristics of Pd/Zr–Al–La catalyst, X-ray fluorescence spectrometer (XRF), Brunauer-Emmett-Teller surface area analyzer (BET), Thermogravimetric analysis (TGA), and Fourier transform infrared spectrometer (FTIR) were performed. The effect of various process conditions on

the catalytic activity and selectivity of the trimetallic nanohybrid catalyst in the hydrogenation of EAQ was examined in the high pressure autoclave reactor.

2 Materials and methods

2.1 Chemicals

Alkylanthraquinone derivative as 2-ethyl-9,10-anthraquinone (EAQ, Alfa Aesar), trimethylbenzene (TMB, LOBA Chemie), trioctylphosphate (TOP, Alfa Aesar), zirconium oxychloride ($ZrOCl_2{\cdot}8H_2O$, LOBA Chemie), aluminum chloride ($AlCl_3$, Merck), lanthanum nitrate hexahydrate ($La(NO_3)_3{\cdot}6H_2O$, Merck), and palladium chloride ($PdCl_2$, Sigma Aldrich), were obtained and used as supplied without further purification.

2.2 Preparation of catalyst

The preparation of support was followed as described in the literature (Ingle et al. 2020b). A novel nanohybrid trimetallic catalyst support (Zr–Al–La) was developed using the co-precipitation technique and subsequently impregnated with Pd catalyst using an incipient wetness impregnation method. $ZrOCl_2{\cdot}8H_2O$ (0.5 M), $AlCl_3$ (0.5 M), and $La(NO_3)_3{\cdot}6H_2O$ (0.5 M) were mixed altogether and dissolved to make a mixed solution. The ammonia was added to the solution at the rate of three drops per minute till the pH reaches to 9.5 and allowing the mixed solution to precipitate. The filtrate was centrifuged and washed with millipore water till the pH reduces to 6.5–7. The precipitate was then dried for 72 h at 60 °C in hot air oven before being pulverized into the fine powder using the mortar and pestle. The support was stored in an airtight container at room temperature. The other catalyst supports were synthesized in the same way with various molar ratio concentrations. As alumina is highly porous and provides excellent support for the loading of other metals, it was employed in the synthesis at a concentration similar to the other components. Zirconium, a rare earth metal can support newer metals subjected to economic constraints. Also Lanthanum can be used for catalytic activities to a certain extent.

Pd was incorporated on the support using the incipient wetness impregnation technique. The synthesized support Zr–Al–La was added to 100 mL of $PdCl_2$ aqueous solution at 27 °C for 48 h with continuous stirring at 150 rpm. Ammonia was added dropwise till it attains the pH of 12. Further, it was rinsed with millipore water and centrifuged to achieve a neutral pH of the filtrate, and tested with a 1 wt.% $AgNO_3$ solution before being dried at 120 °C for 6 h. Three further variations of the catalysts were synthesized in the same way with various Pd loading (wt.%) and termed them as 0.3 wt.% PdO/Zr–Al–La, 0.5 wt.% PdO/Zr–Al–La, and 0.7 wt.% PdO/Zr–Al–La. The PdO/Zr–Al–La sample was made by calcining the dried product in the muffle furnace for 2 h in the air at 400 °C. PdO/γ-Al_2O_3 was also synthesized with the same procedure using γ-Al_2O_3 as support. PdO/γ-Al_2O_3 and PdO/Zr–Al–La catalysts were reduced at 200 °C in presence of H_2/Ar for 2 h to obtain Pd/γ-Al_2O_3 and Pd/Zr–Al–La catalysts. It was kept and stored at room temperature in an airtight container. The detailed procedure is shown in Figure 2.

2.3 Hydrogenation of EAQ

The EAQ working solution was obtained by dissolving EAQ in nonpolar solvent TMB and polar solvent TOP in the volume ratio of 1:1. 120 g of solid EAQ was mixed in 500 mL of TOP and 500 mL of TMB to prepare the working solution of EAQ. The hydrogenation reaction was performed in the high pressure stainless steel autoclave reactor at 0.3 MPa and 75 °C. The reduced catalyst was taken in 30 mL of EAQ working solution and mixed with continuous stirring in the autoclave reactor. The initial concentration of EAQ in the working solution with catalyst was 109 g/L. Nitrogen (N_2) was first purged into the reactor to eliminate air. The autoclave reactor was sealed and heated to 75 °C. Once the desired temperature established, the reaction was immediately initiated by replacing the gas phase with H_2. The initial studies were carried out with various stirring speeds to remove the possibility of external mass transfer constraints (in the range of 500–1500 rpm). The results revealed that the conversion remained constant at a stirring speed of 1000 rpm. Therefore, the stirring speed was set to 1000 rpm for all of the experimental runs in this study. The influence of mass transfer on the reaction rate was investigated using various catalyst doses (0.1–0.7 g). The catalyst was reduced with H_2 at 0.3 MPa, 200 °C for 2 h in a high pressure autoclave before being used in the reaction.

The influence of reaction time, pressure, and Pd loading on conversion, hydrogenation efficiency, selectivity, and H_2O_2 yield were investigated. After the hydrogenation, 30 mL of the solution was centrifuged for 5 min at 4000 rpm to isolate the solid catalyst. Thereafter, 2 mL of catalyst free solution (EAHQ) was taken and added to 20 mL of millipore water and oxidized with O_2 for 20 min at atmospheric pressure and room temperature. The concentration of H_2O_2 was determined by mixing 5 mL of 20% H_2SO_4 with 2 mL of the aqueous oxidized solution, and titrating with a $KMnO_4$ solution (Drelinkiewicz et al. 2005, 2007; Drelinkiewicz and Waksmundzka-Gora 2006; Halder and Lawal 2007; Ingle et al. 2020a, 2020b; Ingle, Shende, and Wasewar 2021; Liu et al. 2002; Zhang et al. 2017). The color of the solution can be taken as indiacation to confirm that the oxidation process is complete. To evaluate the concentration of H_2O_2, the resultant solution was extracted twice with distilled water and then titrated with $KMnO_4$ solution in past studies. The conversion of EAQ, yield of H_2O_2, selectivity of EAQ and hydrogenation efficiency are defined as follows (Liu et al. 2002):

$$\text{EAQ Conversion} = \frac{n^t\text{EAQ}}{n^0\text{EAQ}} \times 100\% \tag{1}$$

$$\text{Yield of } H_2O_2 = \frac{n^t H_2O_2}{n^0\text{EAQ}} \times 100\,\%\,, \tag{2}$$

$$\text{EAQ Selectivity} = \frac{n^t\text{EAQ} + n^t H_4\text{EAQ}}{n^0\text{EAQ}} \times 100\,\%\,, \tag{3}$$

$$\text{Hydrogenation efficiency} = \frac{5C_{KMnO_4} \times V_{KMnO_4} \times M_{H_2O_2}}{2V} \tag{4}$$

The concentrations of EAQ and H_4EAQ in the organic phase were determined using an Agilent1200 HPLC system (USA) with the DAD detector (254 nm) and Zorbax C18 column. The mobile phase was consists of a combination of 80% methanol and 20% HPLC water. The sum of moles of EAQ and H_4EAQ was found to be same that the initial

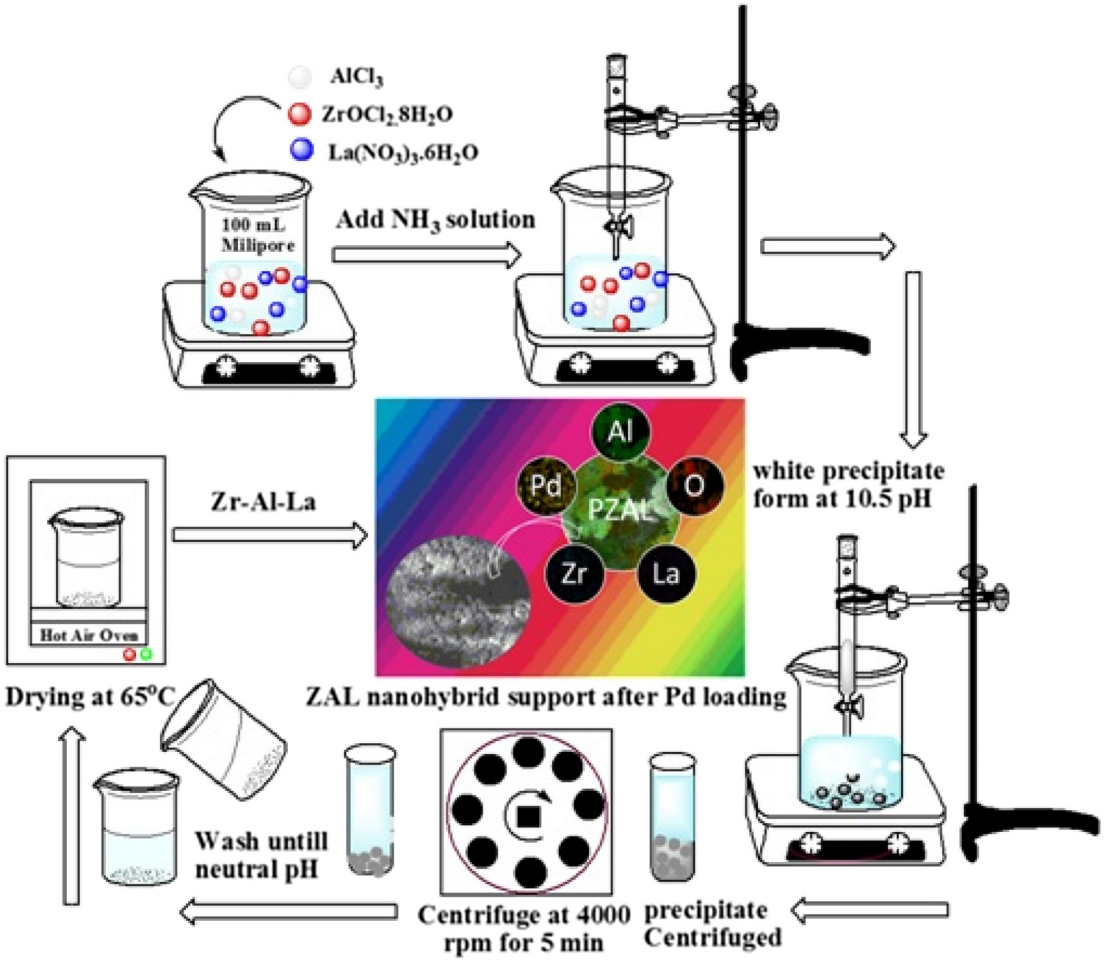

Figure 2: Synthesis of trimetallic nanohybrid catalyst Pd/Zr–Al–La.

moles of EAQ, indicating that no other deep hydrogenated products formed during the experiments.

2.4 Determination of rate controlling step

The main reaction representing the hydrogenation of EAQ is given as follows:

$$\mathrm{EAQ} + \mathrm{H_2} \rightarrow \mathrm{EAHQ} \tag{5}$$

The rate of hydrogenation was studied by measuring the moles of EAQ and H_2 reacted per unit time. The reaction was carried out at 75 °C, 0.3 MPa, and 1000 rpm. At higher stirring speeds, the agitation has no effect on the rate of EAQ and H_2 consumption. Therefore, the overall rate expression can be represented in terms of both the reactants as follows (Levenspiel 1972):

$$-r_A = k_{mn}\left(C_{\mathrm{EAQ}}\right)^m \left(C_{\mathrm{H_2}}\right)^n \tag{6}$$

where, $C_{\mathrm{H_2}} = \frac{P_{\mathrm{H_2}}}{H_r}$.

To validate the first order kinetics, the gaseous reactant is bubbled through a liquid reactant containing suspended catalyst particles in a stirred tank slurry reactor. As the reaction is intended to take place at the surface of catalyst particle, the gaseous reactant must first diffuse through the liquid film to the bulk liquid, and then to the film surrounding the catalyst particle. Therefore, the rate of reaction at the catalyst surface can be equated to the rate of mass transfer through each of the films as follows (Farrauto and Bartholomew 1998):

$$r = r_1 = r_2 = r_3 = r_4 \tag{7}$$

$$r_1 = k_{\mathrm{g}} a_{\mathrm{gl}} \left[\left(P_{\mathrm{H_2}} - P_{\mathrm{H_{2i}}}\right)/H_r \right] \tag{8}$$

$$r_2 = k_{\mathrm{gl}} a_{\mathrm{gl}} \left(C_{\mathrm{H_{2i}}} - C_{\mathrm{H_2}}\right) = k_{\mathrm{gl}} a_{\mathrm{gl}} \left(P_{\mathrm{H_{2i}}} - P_{\mathrm{H_2}}\right)/H_r \tag{9}$$

$$r_3 = k_{\mathrm{ls}} a_{\mathrm{s}} \left(C_{\mathrm{H_2}} - C_{\mathrm{S}}\right) = k_{\mathrm{ls}} a_{\mathrm{s}} \left(P_{\mathrm{H_2}} - P_{\mathrm{S}}\right)/H_r \tag{10}$$

The reaction rate at the surface of the catalyst particle can be estimated as follows:

$$r_4 = k a_{\mathrm{s}} C_{\mathrm{S}} = k a_{\mathrm{s}} P_{\mathrm{S}} \left(\frac{1}{H_r}\right) \tag{11}$$

where k denotes first order rate constant for the surface reaction. On combining equations (8)–(11) at the steady state condition, C_S and C_l can be eliminated and rewritten as:

$$r = \frac{P_{H_2}}{\left[\left(\frac{1}{k_g a_{gl}} + \frac{1}{k_{gl} a_{gl}} + \frac{1}{k_{ls} a_s} + \frac{1}{k a_s}\right) H_r\right]} \quad (12)$$

As H_2 is a pure gas that diffuses quickly through gas film, therefore the gas film resistance can be neglected. Thus, the reaction rate can be written as:

$$r = \frac{P_{H_2}}{\left[\left(\frac{1}{k_{gl} a_{gl}} + \frac{1}{k_{ls} a_s} + \frac{1}{k a_s}\right) H_r\right]} \quad (13)$$

On rearranging equation (13);

$$\frac{P_{H_2}}{r} = \left(\frac{H_r}{k_{gl}}\right)\left(\frac{1}{a_{gl}}\right) + \left(\frac{H_r}{k_{ls}} + \frac{H_r}{k}\right)\left(\frac{1}{a_s}\right) = \frac{C_1}{a_{gl}} + \frac{C_2}{a_s} \quad (14)$$

where $C_1 = \frac{H_r}{[k_{gl}]}$ and $C_2 = \left(\frac{H_r}{k_{ls}} + \frac{H_r}{k}\right)$.

The effect of stirring speed was studied by keeping the temperature, pressure, and amount of catalyst constant. The stirring promotes mass transfer by reducing bubble size, increasing gas-liquid interfacial area, and reducing the thickness of the liquid film around the H_2 bubbles and catalyst particles. The effect of catalyst surface area (a_s) was evaluated by varying the amount of catalyst at constant temperature, pressure, and stirring speed. The following formula can be used to calculate specific surface area of the catalyst:

$$a_s = m_s\left(\frac{6}{d_p} + \frac{\rho_l}{\rho_p}\right) \quad (15)$$

The rate of reaction can be rewritten with including a_s from equation (15):

$$\frac{1}{r} = C_1' + \frac{C_2'}{m_s} \quad (16)$$

where $C_1' = \frac{H_r}{[k_g a_{gl} P_{H_2}]}$ and $C_2' = \frac{\left(\frac{H_r}{k_{ls}} + \frac{H_r}{k}\right)}{\left[P_{H_2}\left(\frac{6}{d_p}\right)\left(\frac{\rho_l}{\rho_p}\right)\right]}$.

The resistance of the gas-liquid interface can be calculated as $\frac{1}{k_{gl} a_{gl}}$, which is the product of the mass transfer coefficient and the gas-liquid interfacial area, $\left[\frac{1}{k_{ls}} + \frac{1}{k}\right]$ represents the overall reaction resistance.

Thiele modulus determines the pore diffusion resistance causing reduction in reactant concentration through catalyst pores, leading to decrease in the reaction rate. Equation (17) was used to calculate the Thiele modulus for the catalyst utilized in the study (Farrauto and Bartholomew 1998).

$$\phi_s = L\sqrt{\frac{k\rho_p}{D_{eff}}} \quad (17)$$

where, $L = d_p/6$ (m).

Equation (18) can be used to calculate the molecular diffusivity of H_2 (Santacesaria et al. 1994).

$$D_{H_2} = 1.05 \times 10^{-2} \exp\left[\frac{-1520}{T}\right] \quad (18)$$

The effectiveness factor η_s, is the ratio of actual reaction rate in the catalyst particle to the rate with no drop in concentration due to pore diffusion resistance. Equation (19) can be used to compute the effectiveness factor for the first order reaction in terms of H_2 for the corresponding Thiele modulus (Farrauto and Bartholomew 1998).

$$\eta_s = \frac{\tanh \phi_s}{\phi_s} \quad (19)$$

Equation (20) represents the intrinsic rate expression for the hydrogenation of EAQ produced in a stirred tank reactor, excluding any mass transfer constraints (Chen 2001):

$$r_{H_2} = 0.9936 \times 10^{-8} \exp\left(\frac{-17.041}{RT}\right) P_{H_2} \quad (20)$$

3 Results and discussion

3.1 Characterization

The elemental composition of the synthesized Pd catalyst was performed using XRF analysis (Malvern Panalytical Epsilon 3^{XLE} model). The XRF spectrometer can detect elements ranging from fluorine (F) to americium (Am) at concentrations ranging from sub-ppm to 100 wt.%. The elemental analysis of Zr–Al–La and Pd/Zr–Al–La is shown in Table 1. Both the support materials and the catalyst contain significant concentrations of Al_2O_3, ZrO_2, and La_2O_3, as well as other compounds such as PdO (in Pd/Zr–Al–La).

The specific surface area was measured using a NOVA touch 1F with nitrogen adsorption-desorption technique and the BET surface area analyzer based on the adsorption isotherm. The specific surface area of Pd supported on trimetallic nanohybrid Zr–Al–La catalyst was determined using the BET equation as follows:

$$\frac{1}{W\left(\frac{P}{P_0} - 1\right)} = \frac{(C-1)}{W_m C}\left(\frac{P}{P_0}\right) + \frac{1}{W_m C} \quad (21)$$

$$W = \frac{V \times M_W}{22.4 \times 1000} \quad (22)$$

Table 2 describes the relative pressure (P/P_0) and volume of gas adsorbed at STP as estimated by equations (21) and (22). As illustrated in Figure 3, plotting $\left(\frac{P}{P_0}\right)$ versus $\frac{1}{W\left(\frac{P}{P_0} - 1\right)}$ using BET equation provides a straight line with the

Table 1: The composition of Zr–Al–La support and Pd/Zr–Al–La catalyst.

Compound	ZrO_2 (%)	Al_2O_3 (%)	La_2O_3 (%)	Other (%)	PdO (%)
Zr–Al–La	43.29	26.37	20.72	9.62	–
Pd/Zr–Al–La	41.67	26.02	26.99	4.80	0.52

Table 2: Relative pressure (P/P_0) and volume of gas adsorbed at STP.

Relative pressure (P/P_0)	Volume adsorbed (cc/g)	Weight of adsorbent (g)	$1/[W(P/P_0 - 1)]$
0.0494	10.3967	0.0130	4.0044
0.1094	12.1359	0.0151	8.0936
0.1714	13.5590	0.0169	12.1988
0.2347	14.8585	0.0185	16.5039
0.2964	16.0509	0.0200	20.9862

slope (S) of $\frac{(C-1)}{W_mC}$ and an intercept (i) of $\frac{1}{W_mC}$. Thus, the specific surface area was calculated to be 146.56 m^2/g.

The FTIR spectra of Pd/Al_2O_3 and the nanohybrid catalyst Pd/Zr–Al–La are shown in Figure 4. The Al–O–Al bond is assigned to the absorbance bands at 477 cm^{-1} in the FTIR spectra of Pd/Al_2O_3, while one low-frequency band at 1640 cm^{-1} is assigned to PdO. The broad band at 3445 cm^{-1} is caused by the stretching vibration of adsorbed water.

The bending vibration of the O–H group accounts for the peak at 1640 cm^{-1} in FTIR spectra of the Zr–Al–La nanohybrid support. The peaks at 739, 614, and 475 cm^{-1} are formed by vibrations of mixed metal oxides. The large peak at 1410 cm^{-1} indicates the bending vibration of Zr–OH groups. The appearance of bands in the support at 739, 1410, and 674 cm^{-1} corresponds to Al–O, Zr–O, and La–O, respectively (Dou et al. 2012; Thanh et al. 2016; Vilas, Philip, and Mathew 2016). The calcination of the prepared catalyst resulted in the formation of oxygen containing functional groups (PdO/Zr–Al–La), whereas the reduction of the catalyst before the hydrogenation reaction resulted in the development of the metallic phase (Pd/Zr–Al–La).

The thermal stability of the Pd/Zr–Al–La nanohybrid catalyst was studied using TGA analysis. The catalyst sample was taken in the sample pan and heated from 30 to 900 °C at the heating rate of 10 °C/min under the nitrogen atmosphere. The TGA thermogram of Pd/Zr–Al–La is shown in Figure 5. The elimination of physically attached water molecules caused about 25% weight loss in the first stage of heating in the temperature range of 100–200 °C. However, about 47% weight loss was recorded in the second stage between 200 and 600 °C. It is associated with the reduction of crystallization water and low molecular weight compounds (Mohan et al. 2016). The actual degradation of catalyst material starts at the temperature of around 100 °C and almost gets stabilized at the temperature of around 600 °C. Therefore, based on the thermogravimetric analysis, it can be said that the synthesized catalyst is thermally stable up to the temperature of around 100 °C. There is no substantial loss resulting above the temperature of 600–900 °C. Hence, the Pd/Zr–Al–La nanocatalyst can be used efficiently for hydrogenation reactions, as the majority of the hydrogenation of EAQ is carried out below 100 °C.

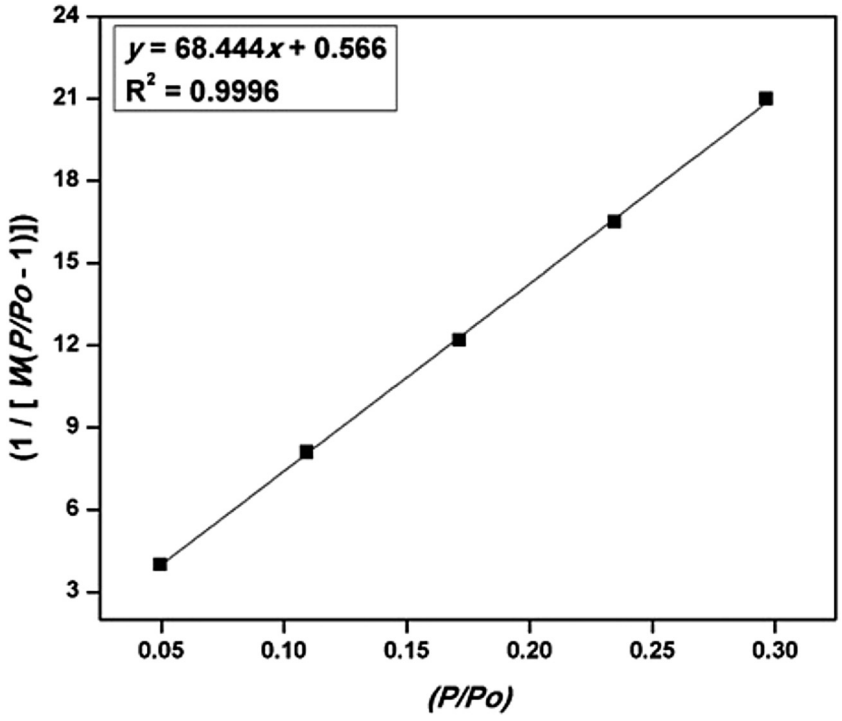

Figure 3: Adsorption isotherm of N_2 for Pd/Zr–Al–La catalyst.

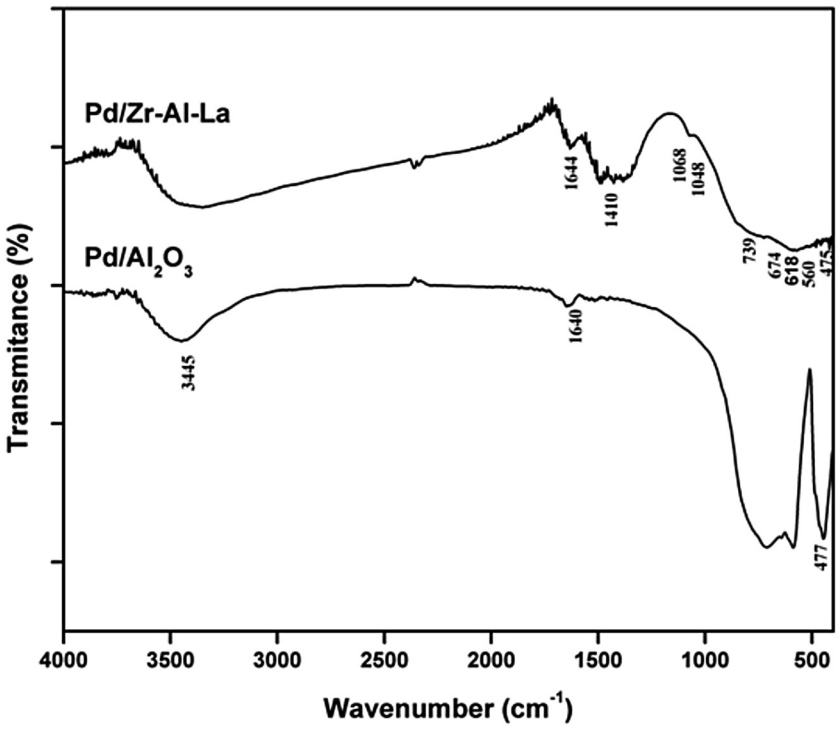

Figure 4: FTIR spectrum of Pd/Al_2O_3 and Pd/Zr–Al–La catalyst.

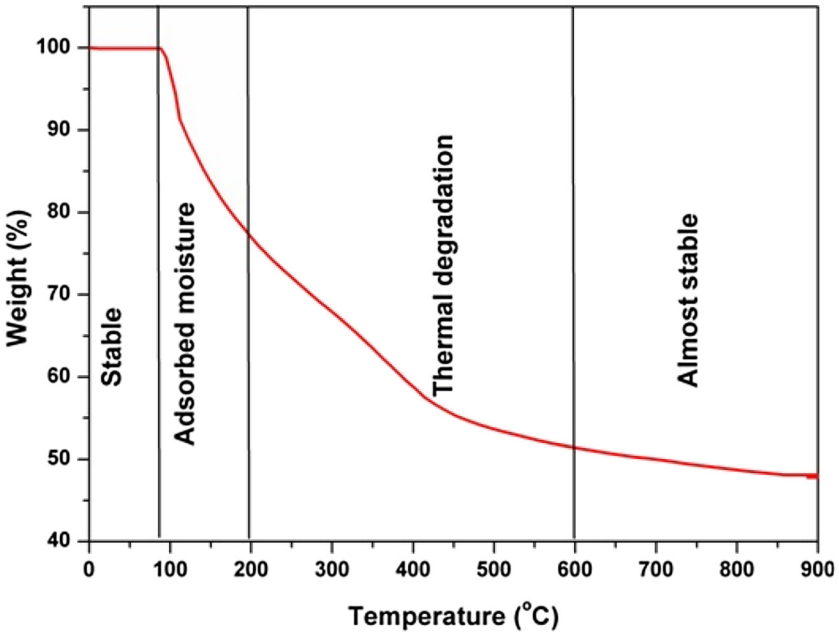

Figure 5: TGA analysis of Pd/Zr–Al–La catalyst.

3.2 Catalytic performance test

3.2.1 Effect of reaction time

The experiments on catalytic hydrogenation were carried out in the high pressure autoclave reactor using a Pd/Zr–Al–La catalyst to investigate the reaction kinetics of EAQ hydrogenation. The hydrogenation of EAQ using the Pd/Zr–Al–La catalyst is zero order in terms of EAQ concentration and first order in terms of H_2 concentration (According to the integral method of analysis) (Berglin and Schoon 1981; Santacesaria et al. 1994, 1999). Figure 6 confirms the zero order of the reaction with respect to concentrations of EAQ. However, the hydrogenation behavior of EAQ in the initial stage differs from that in the deep hydrogenation stage (Drelinkiewicz 1995).

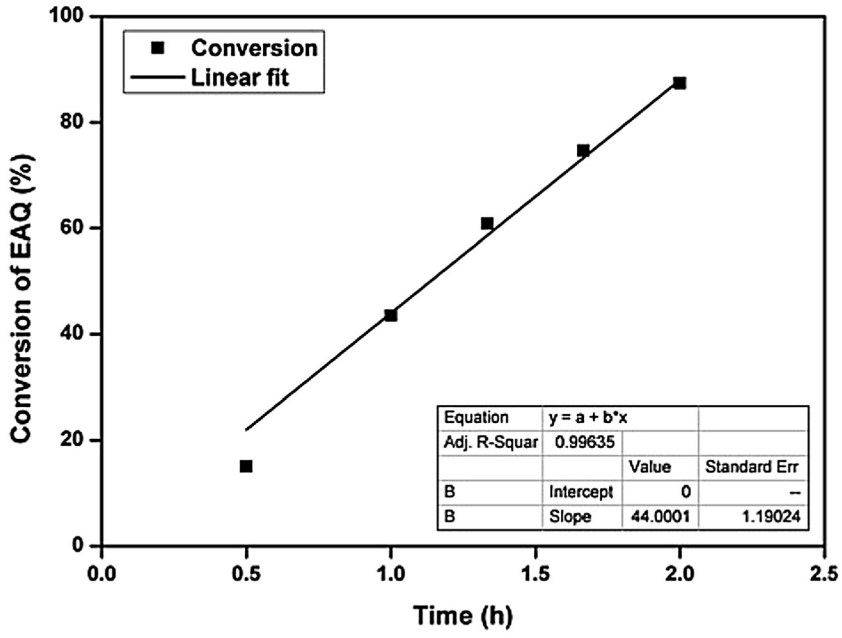

Figure 6: Conversion of EAQ vs. reaction time (Reaction conditions: Temperature = 75 °C, pressure = 0.3 MPa, initial concentration of EAQ = 109 g/L, volume of WS = 30 mL, and catalyst dose = 0.5 g).

The rate of liquid-phase hydrogenation using Pd/Zr–Al–La catalyst for EAQ conversion (r_{EAQ}), EAHQ formation (r_{EAHQ}), and hydrogen consumption (r_{H_2}) was determined with varying catalyst doses. The r_{EAQ}, r_{H_2}, and r_{EAHQ} values were determined using the slope of the reactant and product concentrations plot per unit time. The rate of reaction of the zero order reaction is equal to the rate constant and remains constant during the reaction period. As shown in Figure 7, the rate of EAQ conversion is nearly constant throughout the reaction at various catalyst doses. The rate of first order reaction drops as the concentration of H_2 in the reaction lowers. As shown in Figure 7, the rate of H_2 consumption decreases with the reaction time. The rate of formation of the EAHQ decreases as the overall order of the reaction becomes first order.

3.2.2 Effect of hydrogen pressure

The kinetic rate model was developed to explore the impact of changing EAQ concentration on reaction rate. With increasing EAQ concentrations, the catalytic activity of both Pd/Al_2O_3 and Pd/Zr–Al–La catalysts is almost constant. It confirms that EAQ conversion is virtually zero order dependent on EAQ concentration (Figure 8). In the liquid-phase hydrogenation of EAQ, the rate of reaction for hydrogen was calculated using the concentration of consumed hydrogen. At constant temperature, Henry's law states that the consumed hydrogen concentration is proportionate to the hydrogen pressure. Therefore, the experiments were carried out to investigate the influence of varying H_2 pressure on EAQ conversion. As shown in Figure 9, the conversion of EAQ is proportional to H_2 pressure using both Pd/Al_2O_3 and Pd/Zr–Al–La catalysts, indicating that the apparent reaction orders for H_2 of Pd/Al_2O_3 and Pd/Zr–Al–La catalysts are nearly first order (Hong et al. 2017).

3.2.3 Effect of Pd loading

The effect of Pd loading was studied on the catalyst activity and selectivity at constant temperature (75 °C), pressure (0.3 MPa), and reaction time (2.33 h) with the initial concentration of EAQ of 109 g/L. The catalyst was prepared with 0.3, 0.4, 0.5, and 0.6 wt.% Pd loading. The catalyst activity and selectivity were found to be relatively higher using 0.5 wt.% Pd loading catalyst than that of the catalyst with other variations of Pd loading i.e. 0.3, 0.4, and 0.6 wt.%. The Pd particles were not detected in the XRD analysis in the case of 0.3 and 0.4 wt.% Pd loading catalysts, therefore, the reactants could not access them more easily. At the Pd loading of 0.5 wt.%, Pd particles emerge on the outer surface of the nanohybrid support and it could have enabled by the accessible reactants. The higher Pd loading (0.6 wt.%) could not enhance the net active sites and instead resulted in larger Pd particles on the outer surface of the support. Thus, the catalyst activity could not be increased with Pd loading more than 0.5 wt.%. The selectivity of the catalyst was found to be constant at various Pd loading as shown in Figure 10.

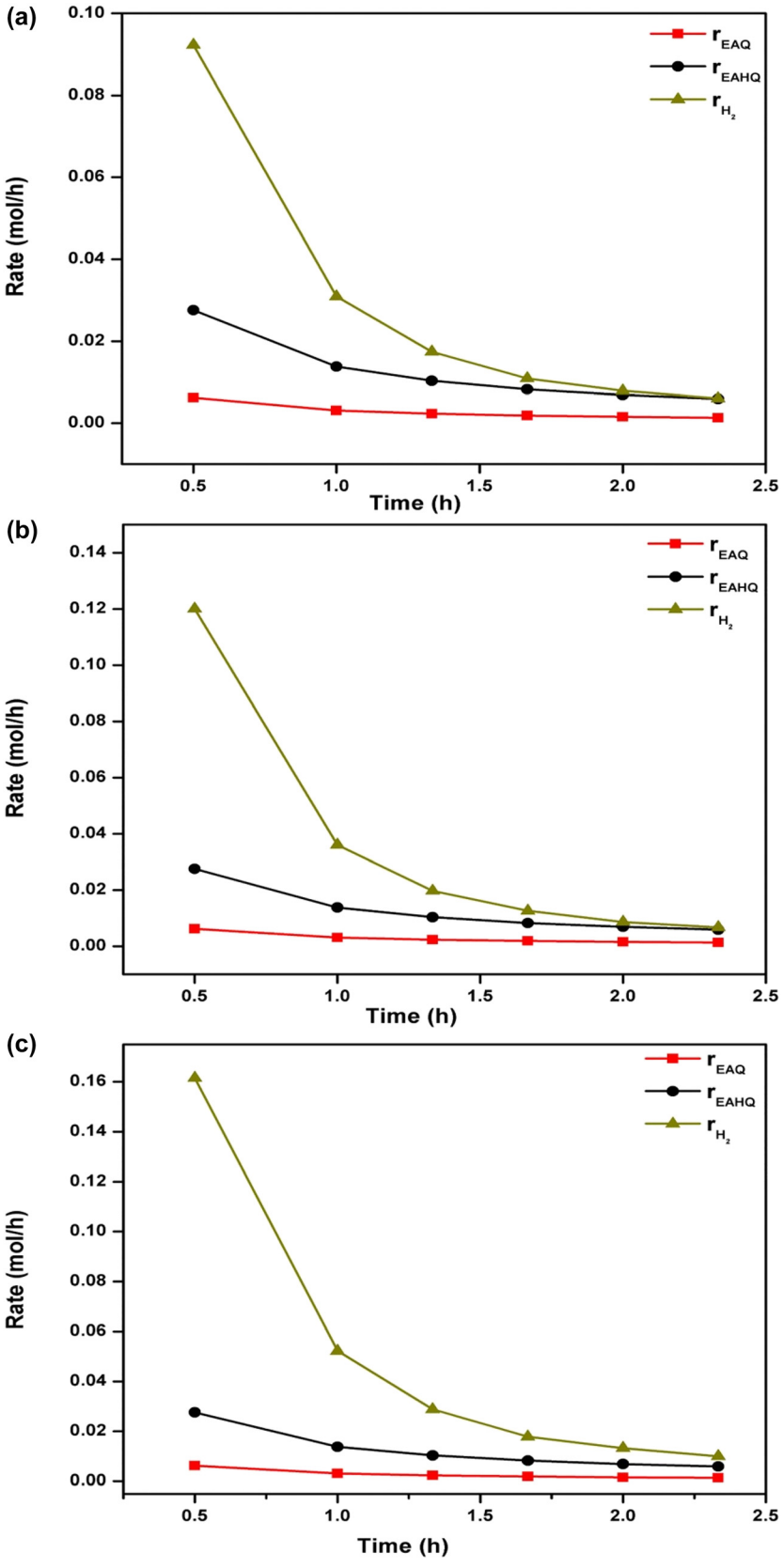

Figure 7: Rates of EAQ conversion, EAHQ formation and H2 consumption as a function of reaction time (Reaction conditions: Temperature = 75 °C, pressure = 0.3 MPa, initial concentration of EAQ = 109 g/L, volume of WS = 30 mL, and catalyst doses (a) 0.1 g, (b) 0.3 g, and (c) 0.5 g).

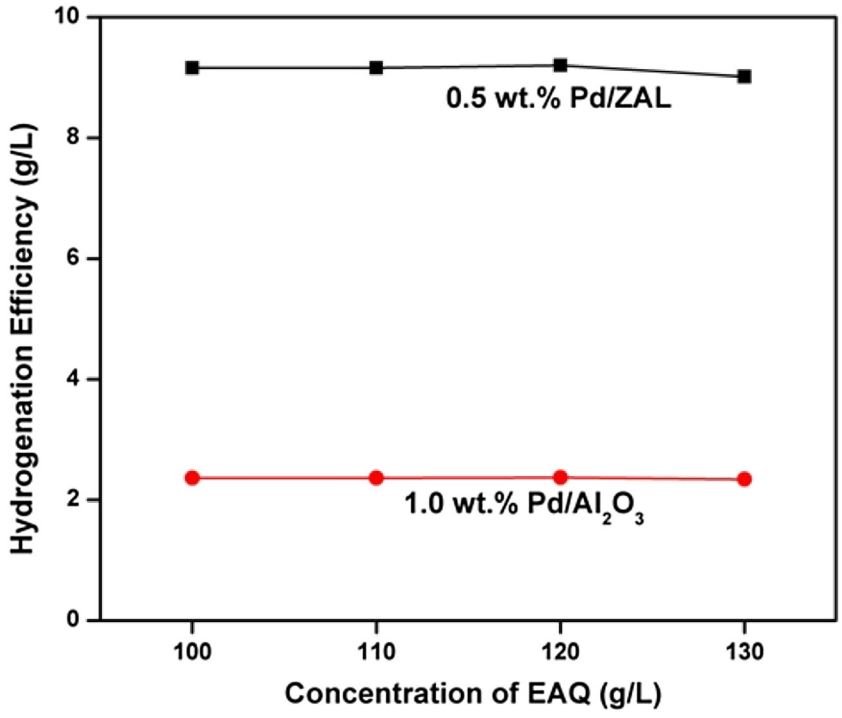

Figure 8: Effect of concentration of EAQ on the hydrogenation efficiency (Reaction conditions: Temperature = 75 °C, pressure = 0.3 MPa, stirring speed = 1000 rpm, catalyst dose = 0.5 g, time = 2.66 h).

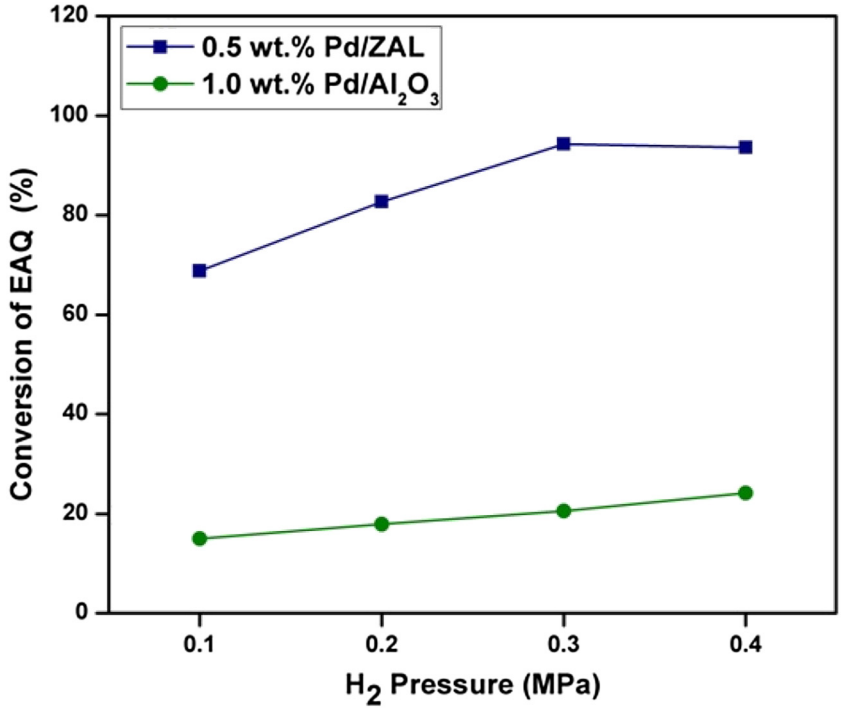

Figure 9: Conversion of EAQ vs.hydrogen pressure (Reaction conditions: Temperature = 75 °C, pressure = 0.3 MPa, stirring speed = 1000 rpm, initial concentration of EAQ = 109 g/L catalyst dose = 0.5 g, time = 2.66 h).

3.2.4 Effect of catalyst doses

The effect of mass transfer on the reaction rate was investigated with varying the catalyst doses (0.1–0.7 g). The influence of catalyst doses on hydrogenation efficiency, conversion, and selectivity was investigated with an initial concentration of EAQ of 109 g/L at a constant temperature (75 °C) and reaction time (2.33 h). The hydrogenation performance found to be enhanced with increase in the catalyst doses. It could be attributed to the more active sites for EAQ to be adsorbed on the supported catalyst surface. The hydrogenation efficiency was 4 g/L

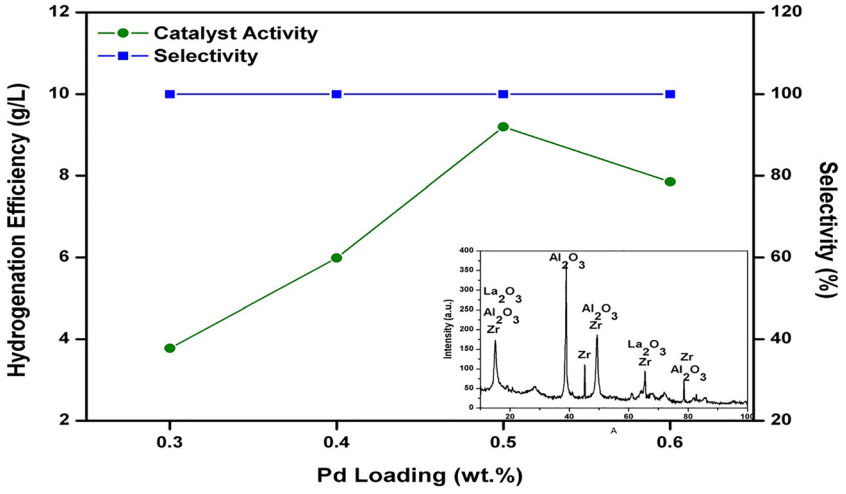

Figure 10: Effect of Pd loading on catalyst activity and selectivity (Indent: XRD spectra for 0.3 and 0.4 wt% Pd loading catalyst) (Reaction conditions: Temperature = 75 °C, pressure = 0.3 MPa, volume of WS = 30 mL, initial concentration of EAQ = 109 g/L).

with a catalyst dose of 0.1 g, and it was increased to 9.15 g/L with a catalyst dose of 0.5 g. It could not significantly improve the hydrogenation efficiency on further increase in the catalyst doses (0.7 g) as shown in Table 3. It was found a linear increase in The hydrogenation rate was observed to be increased with catalyst doses, indicating that the mass transfer does not affect the reaction rate. Thus, it can be concluded that the selectivity of EAQ for the prepared catalyst is desirable. As a result, the hydrogenation of EAQ demonstrates that the Zr–Al–La assisted catalyst can increase the catalyst activity with 100% selectivity for each cycle of hydrogenation of EAQ. The comparison of the performance of 0.5 wt.% Pd/Zr–Al–La catalyst with conventional catalyst (1 wt.% Pd/Al_2O_3) is described in Table 4.

Table 3: Catalytic performance of Pd/Zr–Al–La catalyst for hydrogenation of EAQ.

Catalyst dosage (g)	*E* (g/L)	*S* (%)	*X* (%)
0.1	4.20	100	40
0.3	5.84	100	57
0.5	9.15	100	93
0.7	9.20	100	95

Reaction conditions: Working solution volume:30 mL. Temperature: 75 °C. Pressure: 0.3 MPa. Time: 2.33 h.

Table 4: Comparison with conventional catalytic system.

Sample	*B* (g/L)	*S* (%)	*X* (%)	*R* (%)[a]
1 wt.% Pd/Al_2O_3	2.3	99.4	61	–
0.5 wt.% Pd/Zr–Al–La	9.2	100	95	75

[a]Improvement in hydrogenation efficiency with Pd/Al_2O_3. Reaction conditions: Working solution volume: 30 mL. Catalyst dose: 0.5 g. Temperature: 75 °C. Pressure: 0.3 MPa. Time: 2.66 h.

3.2.5 Effect of pre-treatment of support

It was revealed that the oxidized state of the support and the phase of the active component play an important role in catalytic activity and selectivity during the catalyst synthesis. It was also confirmed from FESEM, XRD, and FTIR analysis that the structure of the prepared catalyst enhances due to the prereatment given viz. calcination and reduction. It is attributed to the pretreatment of the support during catalyst preparation induces oxygen surface, functional groups, making the Pd catalyst more selective. The heat treatment transforms the catalyst into a metallic phase leading to improve in the yield and selectivity. The study demonstrates that the optimum conditions for catalyst preparation are the calcination at 400 °C for 2 h and the reduction at 200 °C, for 2 h.

3.3 Determination of rate controlling step

The mass transfer resistance regulates the reaction rate in the conventional reactor. The mass transfer process gets improved in presence of the catalyst during the hydrogenation of EAQ, allowing the reaction rate to enhanced and reducing the volume of the reactor. Thus, the hydrogenation reaction becomes safer, less expensive, and more environmentally friendly in presence of the catalyst. Equation (15) was used to estimate the intercept C_1', and

found to be 0.033 m^3 s/mol at the stirring speed of 1000 rpm, H_2 pressure of 3 atm, and $1/m_s$ as 5681.82 (Farrauto and Bartholomew 1998).

$$C_1' = \frac{H_r}{[k_{gl}a_{gl}P_{H_2}]} \tag{23}$$

The mass transfer resistance was calculated using equation (23) and found the gas-liquid mass transfer coefficient $k_{gl}a_{gl}$ as 12.89 1/s. The large interfacial area and shorter mass transfer distance produced by the high dispersion may account for the sufficient enhancement of $k_{gl}a_{gl}$. Thus in the catalytic reaction, it leads to effective performance. The gas-liquid mass transfer coefficient was found more than double that of the laboratory trickle bed reactor as $K_{La} \approx 0.01–0.08$ 1/s (AlDahhan et al. 1997).

The specific surface area can be estimated using equation (15) using the values of m_s = 0.01354 $kg_{catalyst}/kg_{liquid}$; d_p, = 5.149 nm; ρ_l, = 1231 kg/m^3; and ρ_p = 2000 kg/m^3 and found to be 4864.12 × 10^3 $m^2_{catalyst}/m^3_{liquid}$.

Equation (17) was used to calculate Thiele modulus of the catalyst used in the study. Equation (24) was used to estimate the values of the rate constant:

$$-r = -\frac{dC}{dt} = k[C_{EAQ}]^0[C_{H_2}]^1 \tag{24}$$

The calculated value of k was 169.23 × 10^{-3} m^3/kg·s. Equation (17) can be used to calculate the molecular diffusivity of H_2. The diffusivity of H_2 was determined to be 0.0133 × 10^{-6} m^2/s at 75 °C. The Thiele modulus was calculated using equation (16), and found to be 0.0136. The effectiveness factor η_s for the first order reaction with respect to H_2 was found to be 0.9999 ≈ 1.0 calculated from the Thiele modulus value.

The intrinsic rate expression for the hydrogenation of EAQ in the stirred tank reactor can be expressed as equation (19), eliminating any mass transfer limitations proposed by Chen (2001). The rate of reaction was calculated using equation (19) and found to be increased to 9.935 × 10^{-9} mol/m^3s, with the addition of a supported Pd/Zr–Al–La catalyst. The particle size, or the dispersion of active metal on the surface of the catalyst support, is essential for improving the catalytic performance. In the hydrogenation of anthraquinone compounds, Al_2O_3 as traditional catalyst support produces the lower yield of 63% and the hydrogenation efficiency of 2.5 g/L with the loss of active quinone compound (Hong et al. 2017). The use of Pd/Zr–Al–La as catalyst improves hydrogenation efficiency (9.15 g/L) and the yield of H_2O_2 (95%) with 100% selectivity. The conversion rate increases with the catalyst dose, demonstrating that mass transfer did not affect the reaction rate. Furthermore, Mears and Weisz-Prater tests were performed on the highest recorded rates to verify any mass transfer limitations identified in the study. The Mears criteria are as follows:

$$C_M = \frac{-r'_{H_2}\rho_b Rn}{k_c C_{Ab}} < 0.15 \tag{25}$$

The value of Mears criterion's, C_M was found to be 9.19 × 10^{-14} for the external diffusion limitations, which is substantially less than 0.15. Also the estimated value of the Weisz-Prater criterion $C_{WP} = \frac{-r'_{H_2}\rho_c R^2}{D_e C_{AS}} < 1$ was 2.98 × 10^{-13}, which is much less than 1.0 for the characteristic of the internal diffusion limitations. Thus, all of the initial experiments and estimates demonstrate that the ensuing rate data have been collected in kinetically controlled regime.

3.4 Stability test

A series of experimental runs were performed to study the stability of the prepared Pd catalyst in the hydrogenation of EAQ. The experimental condition was fixed at reaction temperature 75 °C; pressure 0.3 MPa using the working solution volume of 30 mL. The reaction was conducted for three successive runs with each catalyst lasting for 2.66 h.

There was a negligible loss of Pd content in the Pd/Zr–Al–La catalyst after three successive runs. Table 5 presents the XRF analysis for the Pd contents of Pd/γ-Al_2O_3 and Pd/Zr–Al–La for fresh and spent catalyst after three runs. Compared to the fresh catalysts, the Pd content of Pd/Zr–Al–La was found to be decreased slightly from 0.5 to 0.47 wt.%. In contrast, the Pd content of Pd/γ-Al_2O_3 exhibits a significant decrease in Pd content from 0.55 to 0.4 wt.%, suggesting that Pd/γ-Al_2O_3 tends to aggregate. It can be attributed to the loss of active metal content after

Table 5: Metal contents after three runs of the fresh and used catalysts.

Sample	Pd content (%)[a]	
	Fresh catalysts	Used catalysts
0.5 wt.% Pd/Zr–Al–La	0.5	0.47
1 wt.% Pd/γ-Al_2O_3	0.55	0.41

[a]Determined from XRF analysis.

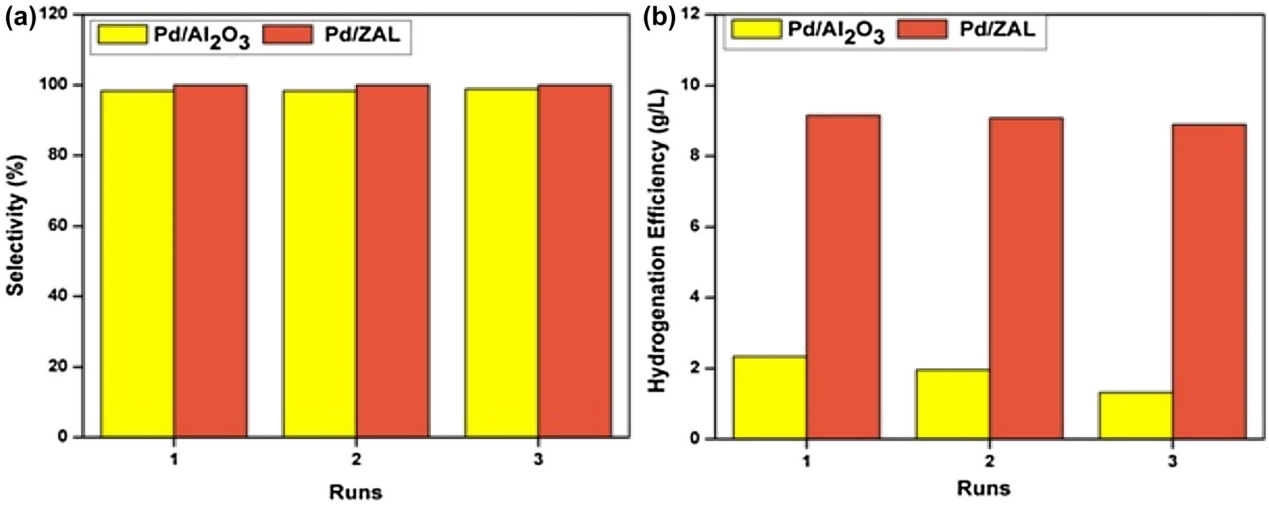

Figure 11: Catalytic performance of catalyst after three runs.

three successive runs, leading to alter the surface area and active sites available for the reaction. It was noticed that only a slight decrease in yield and the hydrogenation efficiency after three runs as compared to that of fresh catalyst as shown in Figure 11.

4 Conclusions

The suitability of catalysts modified with various Pd loadings and prepared using the co-precipitation and impregnation process was explored for the hydrogenation of EAQ. It was concluded that Pd/Zr–Al–La with a Pd loading of 0.5 wt.% provides the highest catalytic activity and selectivity among all modified catalysts. It is also evident from the study that modifying the support increases Pd dispersion, reduces the size of the palladium nanoparticle, and governs the catalyst reducibility. The improved characteristics help the supported Pd based catalyst in the hydrogenation of EAQ to achieve the enhanced catalytic activity. Further, it can be assumed that the requirement of the precious metal (Pd) content in the catalyst used for industrial applications will optimum and significantly reduced. There is a negligible loss in Pd content of the Pd/Zr–Al–La catalyst after the three successive runs indicating the great stability of the prepared catalyst.

The linear relationship between time and initial catalytic activity reveals that the chemical reaction, rather than diffusive mass transport processes, controls the initial hydrogenation rate. The higher catalytic activity of 0.5 wt.% Pd/Zr–Al–La catalyst confirms that the mixed metal oxides effects of Zr, Al, and La enhance the process of hydrogenation of EAQ.

Nomenclature

A_{cs}	adsorbate cross-sectional area (16.2 Å^2/mol for nitrogen)
a_{gl}	gas-liquid interfacial area (m^2/m^3)
a_s	specific surface area of catalyst (m^2/m^3)
C	BET constant
C_{EAQ}	concentration of EAQ (mol/L)
C_{EAQ_0}	initial concentration of EAQ in working solution (mol/L)
C_{H_2}	concentration of H_2 (mol/L)
C_{KMnO_4}	concentration of $KMnO_4$ solution (mol/L)
D_e	effective gas phase diffusivity (m^2/s)
D_{H_2}	molecular diffusivity of H_2 (m^2/s)
d_p	catalyst particle diameter (m)
E	Activation energy (J/mol)
H_r	Henry's constant
k_c	mass transfer coefficient (m/s)
k_g	gas-phase mass transfer coefficients (m/s)
k_{gl}	gas-liquid mass transfer coefficients (m/s)
k_{ls}	liquid-solid mass transfer coefficients (m/s)
$M_{H_2O_2}$	molar mass of hydrogen peroxide (g/mol)

m_s	catalyst loading (kg/m^3)
M_w	molecular weight of the adsorbent gas (Nitrogen = 28.0134 g/mol)
N_{av}	Avogadro's number = 6.023×10^{23} (mol)
n	reaction order
$n^t_{H_2O_2}$	moles of H_2O_2 formed (mol/L)
$n_{0(EAQ)}$	initial moles of EAQ (mol/L)
$n^t_{(EAQ)}$	moles of EAQ at time t (mol/L)
$n^t_{(H_4EAQ)}$	moles of H_4EAQ at time t (mol/L)
P_{H_2}	partial pressure of H_2 (atm)
P/P_0	calculated relative pressure using BET
R	Gas constant, R = 8.314 J/(mol K)
R	catalyst particle radius (m)
r	rate of mass transfer through each film
r_1	rates of mass transfer through the gas film
r_2	rates of mass transfer through gas-liquid interface
r_3	rates of mass transfer through liquid-solid interface
r_4	rates of mass transfer at the surface of the catalyst particle
$-r_{H_2}$	reaction rate for H_2 kmol/kg$_{cat}$ s
$-r_{EAQ}$	EAQ consumption rate (mol/h)
S	selectivity towards active quinone (%)
S_t	total surface area (m^2)
S_p	specific surface area (m^2/g)
T	reaction temperature (°C)
t	reaction time (h)
V_{KMnO_4}	volume of $KMnO_4$ solution (mL)
V	volume of hydrogen peroxide solution (mL)
W	weight of the adsorbed gas (cc/mol)
W_s	weight of the sample (g)
W_t	weight of the adsorbate as a monolayer (g).
x_{EAQ}	conversion of EAQ (%)
$y_{H_2O_2}$	yield of H_2O_2 (%)
η_s	effectiveness factor
ϕ_s	Thiele modulus
ρ_b	bulk density of catalyst (kg/m^3)
ρ_p	catalyst density (kg/m^3)
ρ_l	density of EAQ (kg/m^3)

Author contributions: All the authors have accepted responsibility for the entire content of this submitted manuscript and approved submission.

Research funding: None declared.

Conflict of interest statement: There is no potential conflict of interest to report.

References

Adams, R. D., E. M. Boswell, B. Captain, A. B. Hungria, P. A. Midgley, R. Raja, and J. M. Thomas. 2007. "Bimetallic Ru–Sn Nanoparticle Catalysts for the Solvent-Free Selective Hydrogenation of 1,5,9-Cyclododecatriene to Cyclododecene." *Angewth Chemie International Edition* 46(43):8182–5.

Al-Dahhan, M. H., F. Larachi, M. P. Dudukovic, and A. Laurent. 1997. "High-Pressure Trickle-Bed Reactors: A Review." *Industrial & Engineering Chemistry Research* 36 (8):3292–314.

Berglin, T., and N. H. Schoon. 1981. "Kinetic, and Mass Transfer Aspects of the Hydrogenation Stage of the Anthraquinone Process for Hydrogen Peroxide Production." *Industrial and Engineering Chemistry Process Design and Development* 20 (4): 615–21.

Campos-Martin, J. M., G. Blanco-Brieva, and J. L. G. Fierro. 2006. "Hydrogen Peroxide Synthesis: An Outlook Beyond the Anthraquinone Process." *Angewth Chemie International Edition* 45 (42):6962–84.

Carvalho, L. S., C. L. Pieck, M. C. Rangel, N. S. Figoli, C. R. Vera, and J. M. Parera. 2004. "Trimetallic Naphtha Reforming Catalysts." *Applied Catalysis A: General* 269 (1-2):105–16.

Chen, A., Q. Zhu, Y. Zhao, Y. Tastumi, and T. Iyoda. 2013. "Novel Catalysts of Au/SiO_2 Hybrid Nanorod Arrays for the Direct Formation of Hydrogen Peroxide." *Particle & Particle Systems Characterization* 30(6):489–93.

Chen, H., D. Huang, X. Su, J. Huang, X. Jing, M. Du, D. Sun, L. Jia, and Q. Li. 2015, "Fabrication of Pd/γ-Al_2O_3 Catalysts for Hydrogenation of 2-Ethyl-9,10-Anthraquinone Assisted by Plant-Mediated Strategy." *Chemical Engineering Journal* 262:356–63.

Chen, Q. 2001. "Reviews on the Hydrogenation Kinetics for the Preparation of Hydrogen Peroxide by Anthraquinone Process." *Inorganic Chemical Industry* 33 (2):20–2.

Cheng, Y., L. Wang, S. Lu, Y. Wang, Z. T. Mi. 2008. "Gas-Liquid-Liquid Three-Phase Reactive Extraction for the Hydrogen Peroxide Preparation by Anthraquinone Process." *Industrial & Engineering Chemistry Research* 47 (19):7414–8.

Dou, X., D. Mohan, C. U. Pittman, and S. Yang. 2012. "Remediating Fluoride from Water Using Hydrous Zirconium Oxide." *Chemical Engineering Journal* 198 (198-199):236–45.

Drelinkiewicz A. 1995. "Kinetic Aspects in the Selectivity of Deep Hydrogenation of 2-Ethylanthraquinone Over Pd/SiO_2." *Journal of Molecular Catalysis A: Chemical* 101:61–7.

Drelinkiewicz, A., and A. Waksmundzka-Gora. 2006. "Hydrogenation of 2-Ethyl-9,10-Anthraquinone on Pd/SiO_2 Catalysts: The Role of Humidity in the Transformation of Hydroquinone Form." *Journal of Molecular Catalysis A: Chemical* 258 (1-2):1–9.

Drelinkiewicz, A., A. Waksmundzka-Gora, J. W. Sobczak, and J. Stejskal. 2007. "Hydrogenation of 2-Ethyl-9,10-Anthraquinone on Pd-Polyanaline (SiO_2) Composite Catalyst. Effect of Humidity." *Applied Catalysis A: General* 333 (2): 219–28.

Drelinkiewicz, A., A. Waksmundzka-Gora, W. Makowski, and J. Stejskal. 2005. "Pd/polyaniline(SiO_2) a Novel Catalyst for the Hydrogenation of 2-Ethylanthraquinone." *Catalysis Communications* 6 (5):347–56.

Fang, J., X. Chen, B. Liu, S. Yan, M. Qiao, H. Li, H. He, and K. Fan. 2005. "Liquid-Phase Chemoselective Hydrogenation of 2-Ethylanthraquinone over Chromium-Modified Nanosized Amorphous Ni–B Catalysts." *Journal of Catalysis* 229(1):97–104.

Farrauto, R. J., and C. H. Bartholomew. 1998. "Fundamentals of Industrial Catalytic Processes." *Blackie Academic and Professional* 46:496–504.

Gabriele, C., D. Roland, P. Siglinda, and R. Martin. 2003. "Tubular Inorganic Catalytic Membrane Reactors: Advantages and Performance in Multiphase Hydrogenation Reactions." *Catalysis Today* 79:139–49.

Garcia-Serna, J., T. Moreno, P. Biasi, M. J. Cocero, J. P. Mikkola, and T. P. Salmi. 2014. "Engineering in Direct Synthesis of Hydrogen Peroxide: Targets, Reactors, and Guidelines for Operational Conditions." *Green Chemistry* 16 (5):2320–43.

Gema, B. B., M. Montiel-Argaiz, F. Desmedt, P. Miquel, M. C. M. Jose, and L. G. F. Jose. 2016. "Direct Synthesis of Hydrogen Peroxide with No Ionic Halides in Solution." *RSC Advances* 6 (101): 99291–6.

Halder, R., and A. Lawal. 2007. "Experimental Studies on Hydrogenation of Anthraquinone Derivative in a Microreactor." *Catalysis Today* 125:48–55.

Han, Y., Z. He, S. Wang, W. Li, and J. Zhang.2015. "Performance of Facet-Controlled Pd Nanocrystalsin 2-Ethylanthraquinone Hydrogenation." *Catalysis Science and Technology* 5 (5): 2630–9.

Hong, R., Y. He, J. Feng, and D. Li. 2017. "Fabrication of Supported Pd-Ir/Al_2O_3 Bimetallic Catalysts for 2-Ethylanthraquinone Hydrogenation." *AIChE Journal* 63 (9):3955–65.

Hou, Y., Y. Wang, F. He, W. Mi, Z. Li, Z. Mi, and E. Min. 2004. "Effects of Lanthanum Addition on Ni-B/γ-Al_2O_3 Amorphous Alloy Catalysts Used in Anthraquinone Hydrogenation." *Applied Catalysis A: General* 259 (1):35–40.

Hungria, A. B., R. Raja, R. D. Adams, B. Captain, J. M. Thomas, P. A. Midgley, V. Golovko, and B. F. G. Johnson. 2006. "Single-step Conversion of Dimethyl Terephthalate into Cyclohexanedimethanol with Ru5PtSn, a Trimetallic Nanoparticle Catalyst." *Angewth Chemie International Edition* 45 (29):4782–5.

Ingle, A. A., S. Z. Ansari, D. Z. Shende, K. L. Wasewar, and A. B. Pandit. 2020a. "Hydrogenation of 2-Ethylanthraquinone with Pd Supported on Hollow Ceramic Microsphere Catalyst: An Experimental and Kinetic Study." *Journal of the Indian Chemical Society* 97 (7):1033–7.

Ingle, A. A., S. Z. Ansari, D. Z. Shende, K. L. Wasewar, and A. B. Pandit. 2020b. "Palladium Supported on Nano-Hybrid Zr–Al–La Catalyst for Hydrogenation of 2-Ethylanthraquinone." *Indian Chemical Engineer* 63 (4):387–401.

Ingle, A. A., D. Z. Shende, and K. L. Wasewar. 2021. "Synthesis, Characterization, and Application of Hollow Ceramic Microsphere Based Pd Catalyst for Hydrogenation of 2-Ethylanthraquinone." *Journal of the Indian Chemical Society* 98:100177–87.

Levenspiel, O., 1972. *Chemical Reaction Engineering*, 3rd ed. New York: Wiley.

Li, W., F. Wang, X. Zhang, M. Sun, J. Hu, Y. Zhai, H. Lv, G. Lv. 2021."Highly Dispersed Pd Nanoparticles Supported on γ-Al_2O_3 Modified by Minimal 3-Aminopropyltriethoxysilane as Effective Catalysts for 2-Ethyl-Anthraquinone Hydrogenation." *Applied Catalysis A: General* 619:118–24.

Liew, K. H., T. K. Lee, M. A. Yarmo, K. S. Loh, A. F. Peixoto, C. Freire, and R. M. Yusop. 2019. "Ruthenium Supported on Ionically Cross-Linked Chitosan-Carrageenan Hybrid $MnFe_2O_4$ Catalysts for 4-Nitrophenol Reduction." *Catalysts*, 9 (3):254–65.

Liu, B., M. Qiao, J. Wang, and K. Fan. 2002. "Highly Selective Amorphous Ni-Cr-B Catalyst in 2-Ethylanthraquinone Hydrogenation to 2- Ethylanthrahydroquinone." *Chemical Communications* 2002 (11):1236–7.

Ma, Q., N. Wang, G. Liu, and L. Wang. 2019. "Enhanced Performance of Pd Nanoparticles on SBA-15 Grafted with Alkyltrialkoxysilane in 2-Ethyl-Anthraquinone Hydrogenation." *Microporous and Mesoporous Materials* 279:245–51.

Melada, S., R. Rioda, F. Menegazzo, F. Pinna, and G. Strukul. 2006. "Direct Synthesis of Hydrogen Peroxide on Zirconia-Supported Catalysts under Mild Conditions." *Journal of Catalysis* 239: 422–30.

Mohan, S., V. Kumar, D. K. Singh, and S. H. Hasan. 2016. "Synthesis and Characterization of rGO/ZrO_2 Nanocomposite for Enhanced Removal of Fluoride from Water: Kinetics, Isotherm, and Thermodynamic Modeling and its Adsorption Mechanism." *RSC Advances* 6: 87523–38.

Paparatto, G., and R. D'Aloisio. 2003. "Catalyst and Process for the Direct Synthesis of Hydrogen Peroxide." *US Patent* 6630118: 2003–10–7.

Santacesaria, E., M. Di-Serio, A. Russo, U. Leone, and R. Velotti. 1999. "Kinetic and Catalytic Aspects in the Hydrogen Peroxide Production via Anthraquinone." *Chemical Engineering Science* 54 (13–14):2799–806.

Santacesaria, E., M. Di-Serio, R. Velotti, and U. Leone. 1994. "Kinetics, Mass Transfer and Palladium Catalyst Deactivation in the Hydrogenation." *Industrial & Engineering Chemistry Research* 33 (2):277–84.

Shen, C., Y. J. Wang, J. H. Xu, Y. C. Lu, and G. S. Luo. 2011. "Preparation and the Hydrogenation Performance of a Novel Catalyst-Pdnanoparticle Loaded on Glass Beads with an Egg–Shell Structure." *Chemical Engineering Journal* 173:226–32.

Surisetty, V. R., A. K. Dalai, and J. Kozinski. 2010. "Intrinsic Reaction Kinetics of Higher Alcohol Synthesis from Synthesis Gas over a Sulfided Alkali-Promoted Co–Rh–Mo Trimetallic Catalyst Supported on Multiwalled Carbon Nanotubes (MWCNTs)." *Energy & Fuels* 24 (8):4130–7.

Tan, J., J. Zhang, Y. Lu, J. Xu, and G. Luo. 2012. "Process Intensification of Catalytic Hydrogenation of Ethylanthraquinone with Gas-Liquid Microdispersion." *AIChE Journal* 58 (5):1326–35.

Tang, P., Y. Chai, J. Feng, Y. Feng, Y. Li, and D. Li. 2014. "Highly Dispersed Pd Catalyst for Anthraquinone Hydrogenation Supported on Alumina Derived from a Pseudoboehmite Precursor." *Applied Catalysis A: General* 469:312–9.

Thanh, D. N., Z. Bastl, K. Cerna, P. Ulbrich, and J. Lederer. 2016. "Amorphous Nanosized Al–Ti–Mntrimetal Hydrous Oxides: Synthesis, Characterization and Enhanced Performance in Arsenic Removal." *RSC Advances* 6 (103):100732–42.

Toshima, N., R. Ito, T. Matsushita, and Y. Shiraishi. 2007. "Trimetallic Nanoparticles Having an Au-Core Structure." *Catalysis Today* 122 (3-4):239–44.

Trejo, A. C., I. D. Castañeda, A. C. Rodríguez, V. R. Andrade Carmona, M. P. C. Mercado, L. S. Vale, M. Cruz, S. B. Castillero, L. C. Consuelo, and M. D. Silvio. 2021. "Hydrogen Peroxide as an Adjuvant Therapy for COVID-19: A Case Series of Patients and Caregivers in the Mexico City Metropolitan Area." *Evidence-Based Complementary and Alternative Medicine* 2021: 1–12.

Vilas, V., D. Philip, and J. Mathew. 2016. "Facile One-Pot Synthesis of Crystalline Palladium Nanoparticles with Exceptional Catalytic and Antiradical Activities." *Materials Chemistry and Physics* 170: 1–11.

Yao, H., C. Shen, Y. Wang, and G. Luo. 2016. "Catalytic Hydrogenation of 2-Ethylanthraquinone Using an in SituSynthesized Pd Catalyst." *RSC Advances* 6 (28):23942–8.

Yuan, E., C. Wu, G. Liu, and L. Wang. 2016. "One-Pot Synthesis of Pd Nanoparticles on Ordered Mesoporous Al_2O_3 for Catalytic Hydrogenation of 2-Ethyl-Anthraquinone." *Applied Catalysis A: General* 525:119–27.

Yuan, E., C. Wu, X. Hou, M. Dou, G. Liu, G. Li, and L. Wang. 2017a. "Synergistic Effects of Second Metals on the Performance of (Co, Ag, Cu)-Doped Pd/Al_2O_3 Catalysts for 2-Ethyl-Anthraquinone Hydrogenation." *Journal of Catalysis* 347:79–88.

Yuan, E., X. Ren, L. Wang, and W. Zhao. 2017b. "A Comparison of the Catalytic Hydrogenation of 2-amylanthraquinone and 2-ethylanthraquinone over a Pd/Al_2O_3 Catalyst." *Frontiers of Chemical Science and Engineering* 11 (2): 177–84.

Zhang, J., K. Gao, S. Wang, W. Li, and Y. Han. 2017. "Performance of Bimetallic PdRu Catalysts Supported on Gamma-Alumina for 2-Ethylanthraquinone Hydrogenation." *RSC Advances* 7(11): 6447–56.

Zudin, V. V., V. A. Likholobov, and Y. I. Yermakov. 1980. "Catalytic Synthesis of Hydrogen Peroxide from Oxygen and Water in the Presence of Carbon Monoxide and Phosphine Complexes of Palladium." *Kinetics and Catalysis* 20 (6): 1559–600.